NJC

Accepted Manuscript

This is an *Accepted Manuscript*, which has been through the Royal Society of Chemistry peer review process and has been accepted for publication.

Accepted Manuscripts are published online shortly after acceptance, before technical editing, formatting and proof reading. Using this free service, authors can make their results available to the community, in citable form, before we publish the edited article. We will replace this *Accepted Manuscript* with the edited and formatted *Advance Article* as soon as it is available.

You can find more information about *Accepted Manuscripts* in the Information for Authors.

Please note that technical editing may introduce minor changes to the text and/or graphics, which may alter content. The journal's standard Terms & Conditions and the Ethical guidelines still apply. In no event shall the Royal Society of Chemistry be held responsible for any errors or omissions in this *Accepted Manuscript* or any consequences arising from the use of any information it contains.

ROYAL SOCIETY OF CHEMISTRY

www.rsc.org/njc

$CdS/ZnIn_2S_4/TiO_2$ 3D-Heterostructures and Their Photoelectrochemical Properties

Xuehua Yin[a], Pengtao Sheng[a], Fenfen Zhong[a], VanManh Nguyen[a, b], Qingyun Cai[a,*], Craig Grimes[#]

[a] State Key laboratory of Chem/Biosensing and Chemometrics, College of Chemistry and Chemical Engineering, Hunan University, Changsha 410082, China

[b] Faculty of Chemical Technology, Hanoi University of Industry, Hanoi, Viet Nam

[#] Flux Photon Corporation, 620 Hutton Blvd., Raleigh, North Carolina 27303 USA

*To whom correspondence should be addressed.

E-mail: qycai0001@hnu.edu.cn; qycai0002@gmail.com.

ABSTRACT

We describe the synthesis and application of a three-dimensionally (3D) structured CdS quantum dot / $ZnIn_2S_4$ nanosheet / TiO_2 nanotube array ($CdS/ZnIn_2S_4/TiO_2$) heterostructured material architecture. TiO_2 nanotube arrays (TiO_2 NTAs) are used as the synthetic template, subsequently sensitized using hydrothermal and successive ion layer adsorption and reaction (SILAR) techniques. The described synthesis approach offers a powerful technique for designing 3D heterostructure systems.

Under AM1.5G illumination, the 3D $CdS/ZnIn_2S_4/TiO_2$ samples generate a photocurrent of approximately 4.3mA/cm^2, with a photoconversion efficiency of 2%. Samples are tested for their ability to photocatalytically degrade target agents; noteworthy is that after 90 min illumination 100% of 2, 4-dichlorophenoxyacetic acid (2, 4-D) is removed.

***Keywords**:* photoelectrochemical, heterostructure, photocatalytic, CdS, $ZnIn_2S_4$, TiO_2.

Introduction

Photocatalytic degradation of organic pollutants is a topic of ongoing scientific and commercial interest. [1, 2] Over the past decades, a variety of semiconductor photocatalysts have been synthesized and studied, including TiO_2,[3] ZnO,[4] $BiVO_4$,[5] $AgNBO_3$,[6] and $ZnWO_4$.[7] TiO_2[8, 9] offers several advantages over other semiconductors, including low-cost,[10] non-toxicity,[11] and chemical stability,[12] while the nanotube architecture promotes rapid separation of the photo-generated holes and electrons.[13] However, TiO_2 possesses a band gap of 3.2 eV, suitable for absorbing only some 4% of the incident solar spectrum energy. [14-16]

Numerous investigations have sought to maintain the advantages TiO_2 offers while shifting its band gap so as to utilize visible light, which accounts for some 48% of the incident solar energy;[17] such efforts include, but are certainly not limited to metallic or non-metallic doping,[18] and TiO_2 hydrogenation or reduction.[19] Coupling TiO_2 with visible-light semiconductors appears to offer a viable pathway for obtaining an optimal photocatalyst; heterostructures investigated include Ag_2O/TiO_2, NiO/TiO_2, and CeO_2/TiO_2, [20-22] with their physical structures tailored to promote charge separation.[23-24] Semiconductor quantum dots (QDs) such as CdS, [25] CdSe, [26] CdTe [27] and PbS [28] have been grafted onto TiO_2 as sensitizers to enhance photocurrent response, with the QD bandgap tailored by modifying its physical size.[27, 29] Of these binary semiconductors, CdS has attracted considerable attention for photocatalytic applications, including the synthesis and application of CdS/titanate nanotubes,[30] ZnO/CdS heterostructures, [31] CdS/TaON/graphene composites, [32] and CdS/Bi_2WO_6 heterostructures. [29]

Ternary sulfide $ZnIn_2S_4$, as the only member of the AB_2X_4 family semiconductor with a layered structure, has attracted considerable attention due to its potential application in a variety of fields including catalysis, [33, 34] charge storage, [35] photoconduction, [36, 37] and thermoelectricity.[38] Of particular interest is ternary $ZnIn_2S_4$, a chemically stable chalcogenide semiconductor, well suited to visible light absorption. [39] A variety of $ZnIn_2S_4$ hybrid semiconductor heterostructures have been explored in efforts to improve photocatalytic performance.[40-42] For example, multi-walled carbon nanotubes coupled $ZnIn_2S_4$ composites have been used for hydrogen production,[43] while $ZnIn_2S_4$-PVDF-poly-(MMA-co-MAA) composites have been reported to exhibit high photocatalytic activity for degradation of methyl orange.[44]

In an effort to achieve a high performance chemically stable visible light photocatalyst we fabricate $CdS/ZnIn_2S_4/TiO_2$ heterostructures by a facile hydrothermal method coupled with a successive ionic layer adsorption and reaction process (SILAR). We find the $CdS/ZnIn_2S_4/TiO_2$ composites are chemically stable and have excellent visible light photocatalytic properties.

Results and discussion

A high performance visible light photocatalyst, $CdS/ZnIn_2S_4/TiO_2$ heterostructure, was prepared by a facile hydrothermal method coupled with a SILAR technique, as shown in **Fig. 1**. The bandgap of TiO_2 (3.2 eV), $ZnIn_2S_4$ (2.6 eV) and CdS (2.4 eV) reduces progressively with the CB and VB increasing progressively forming a stepwise heterostructure so that the absorption to visible right was significantly enhanced, which was verified in the photodegradation of organic pollutants. The proposed material was first characterized.

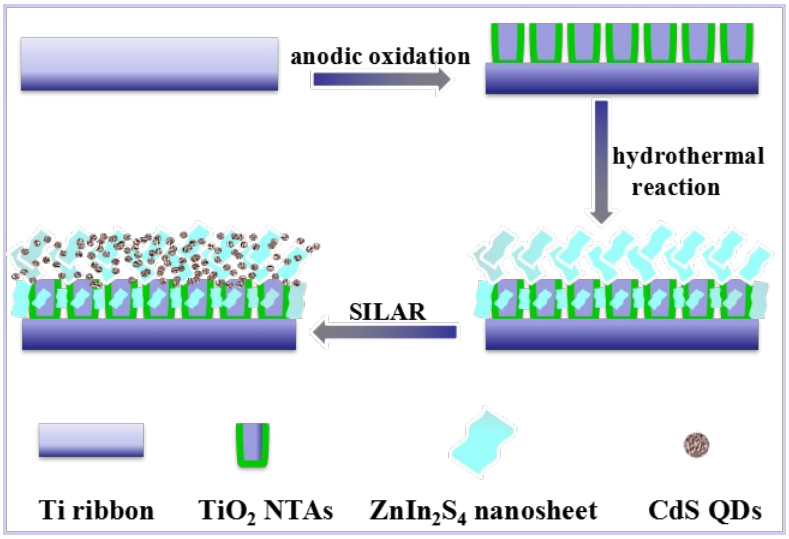

Fig.1. Schematic illustration of the construction of $CdS/ZnIn_2S_4/TiO_2$ heterostructures.

Characterization

Fig. 2 shows SEM images of TiO_2 with/without deposition of $ZnIn_2S_4$ and CdS. The TiO_2 NTAs have an inner pore diameter ranging from 70 to 110 nm and wall thickness of about 15 nm (**Fig. 2A**). The formation mechanism of the TiO_2 NTAs is well documented. [45, 46] As shown in **Fig. 2B**, the surface of the TiO_2 NTAs is homogeneously covered with a 3D layer of dense $ZnIn_2S_4$ nanosheets. **Fig. 2C and 2D** displays the cross-sectional images of unmodified TiO_2 NTAs and $ZnIn_2S_4/TiO_2$ NTAs, respectively. The bare TiO_2 NT is smooth and clean (**Fig. 2C**), while in the $ZnIn_2S_4/TiO_2$ NTAs, the TiO_2 NT is filled with $ZnIn_2S_4$ nanosheets (**Fig. 2D**). The tubular space limited the size of $ZnIn_2S_4$, no flower-like $ZnIn_2S_4$ was formed. The $ZnIn_2S_4$ nanosheets are distributed randomly on the surface and interstices of nanotubes, and the gap between TiO_2 NTs almost disappears owing to the filling of $ZnIn_2S_4$ nanosheets. **Fig. 2E** shows the image of $ZnIn_2S_4$ nanosheets remaining in solution after hydrothermal reaction, which already self-assembled into

microspheres. After 5 cycles' CdS absorbed onto $ZnIn_2S_4/TiO_2$ heterostructure, the surface of the material (**Fig. 2F**) becomes a little rougher than undecorated $ZnIn_2S_4/TiO_2$ (**Fig. 2B**). As can be seen in the inset of **Fig. 2F**, with further increasing the amount of CdS, a rather rougher surface would be gained, thus, small particles of CdS grow into larger crystals.

Fig. 2G and **2H** show the EDS of the selected area in $ZnIn_2S_4/TiO_2$ and $CdS/ZnIn_2S_4/TiO_2$, respectively. The EDS analysis of **Fig. 2G** shows the characteristic peaks of Zn, In and S with an approximate elemental composition of 1:2:4 (Zn/In/S), and the characteristic peaks of Ti and O with an approximate elemental composition of 1:2 (Ti/O), redundant Ti belongs to the Ti substrate, verifying the desired stoichiometry of the heterostructure $ZnIn_2S_4/TiO_2$. Moreover, in **Fig. 2H**, we can see that the calculated molar percentages of Zn, In, S and Cd are about 8.06%, 17.74 %, 38.08 % and 4.31 %, respectively, corresponding to the molar ratio of 1:2:4.5:0.5(Zn/In/S/Cd), which verified the desired stoichiometry of the heterostructure $CdS/ZnIn_2S_4/TiO_2$.

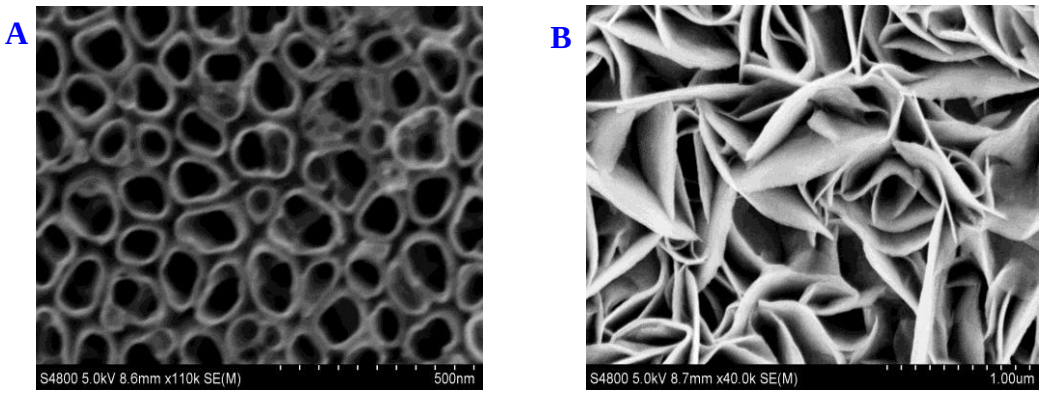

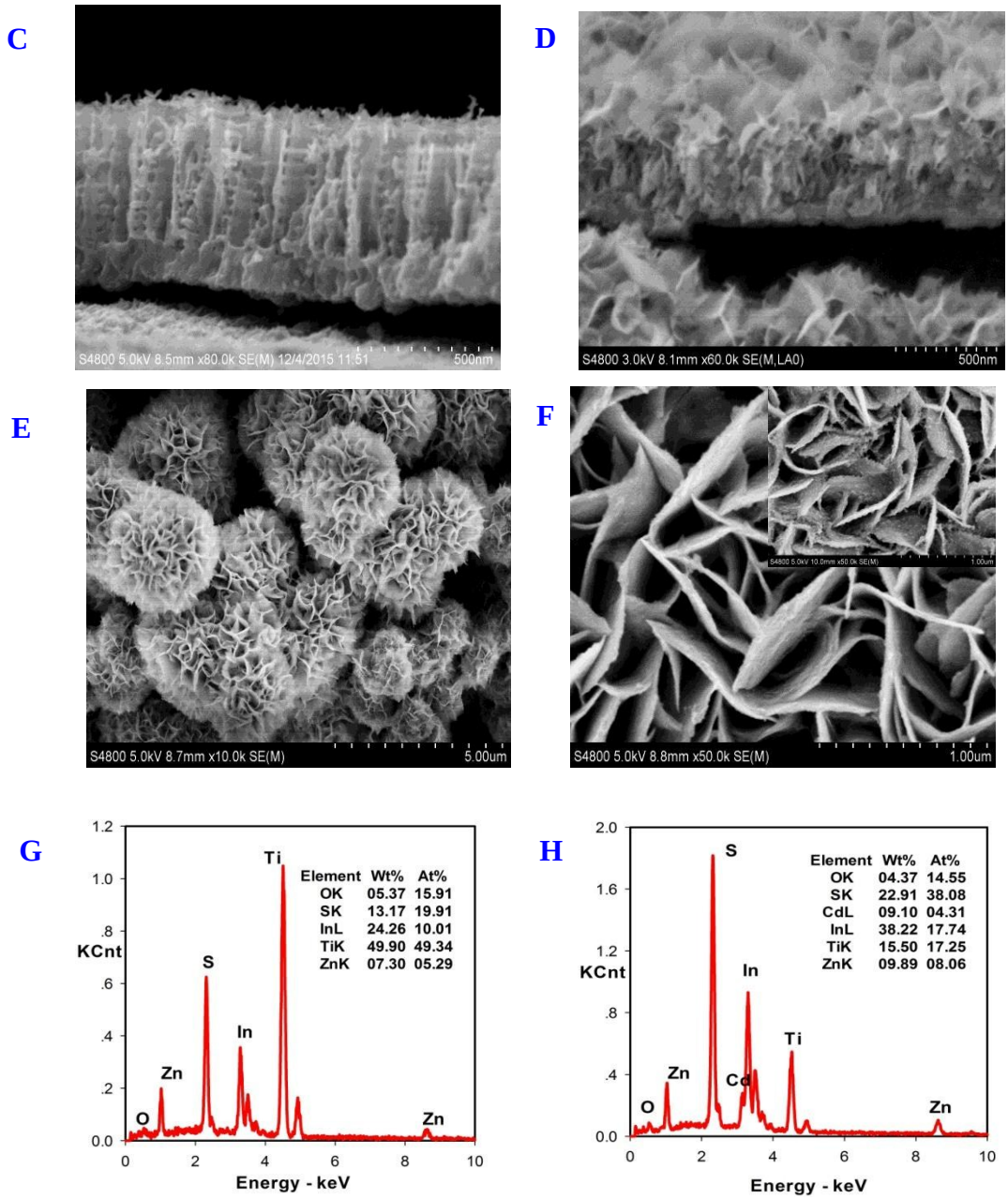

Fig.2. SEM of TiO_2 nanotube arrays (A), top view of $ZnIn_2S_4/TiO_2$ heterostructure (B), sectional view of TiO_2 NTAs (C) and $ZnIn_2S_4/TiO_2$ heterostructure (D), self-assembled $ZnIn_2S_4$ nanosheets in the solution of hydrothermal synthesis process (E), $ZnIn_2S_4/TiO_2$ heterostructure deposited with CdS 5 cycles (F), 9 cycles (the inset of F), the corresponding EDS of $ZnIn_2S_4/TiO_2$ heterostructure (G) and $CdS/ZnIn_2S_4/TiO_2$ (H).

UV-Vis diffuse reflectance spectra of the electrode materials are shown in **Fig. 3**, which is consistent with the results previously reported.[47-50] We can see that $ZnIn_2S_4/TiO_2$ sample results in a red shift of the absorption peaks, suggesting that the combination of $ZnIn_2S_4$ nanosheets for TiO_2 NTAs can expand the absorption range of photoelectrodes. What's more, $CdS/ZnIn_2S_4/TiO_2$ showed a further red shift. The narrow band-gap of CdS QDs is responsible for the improved absorption capability of $ZnIn_2S_4/TiO_2$ in the visible-light region.

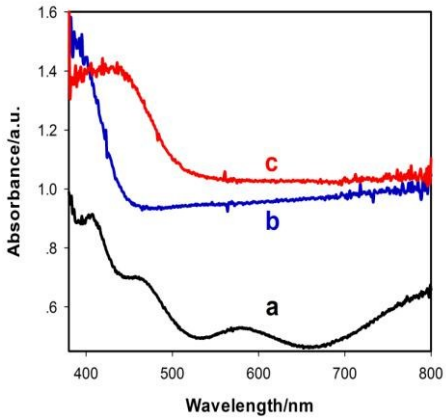

Fig.3. UV-Vis absorption spectra of (a) TiO_2, (b) $ZnIn_2S_4/TiO_2$ and (c) $CdS / ZnIn_2S_4/ TiO_2$.

Photoelectrochemical properties

Photocurrent density-voltage characteristics of the samples were investigated in an electrolyte containing 0.24 M Na_2S and 0.35 M Na_2SO_3 to examine the photoelectrochemical properties. As shown in **Fig. 4**, the photocurrent densities of both the $CdS/ZnIn_2S_4/TiO_2$ and $CdS/ZnIn_2S_4/TiO_2$ materials are much higher than the pure TiO_2 (**Fig. 4A**). **Fig. 4B** shows the time-dependent photocurrent responses of the $CdS/ZnIn_2S_4/TiO_2$ and unmodified TiO_2 NTs under

illumination of 100 mW/cm^2 visible light. Both show the high stability, the photocurrent decreases by 3.02 % within 1 h.

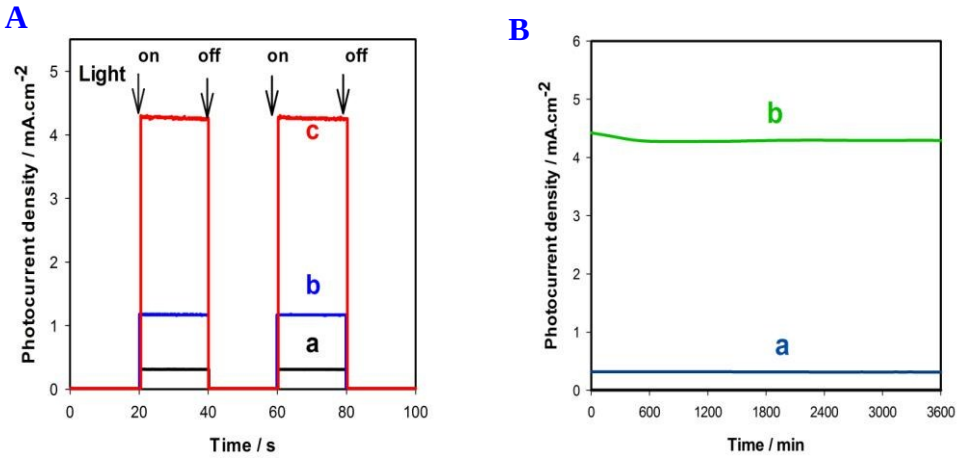

Fig.4. (A) Photocurrent responses of (a) TiO_2, (b) $ZnIn_2S_4$/ TiO_2 and (c) CdS/ $ZnIn_2S_4$/ TiO_2; (B) Time-dependent photocurrent response of: (a) unmodified TiO_2 and (b) CdS/ $ZnIn_2S_4$/ TiO_2.

The photocurrent-applied potential relationship (J-V) is shown in the **Fig. 5A**. The corresponding light to chemical energy conversion efficiencies are shown in **Fig. 5B**, which are calculated as follows: [51-53]

$$\eta(\%) = (total\ power\ output - electrical\ power\ input)/light\ power\ input \times 100$$
$$= j_p\left[E^0_{rev} - |E_{app}|\right]/I_0 \times 100 \quad (1)$$

where j_p is the photocurrent density (mA/cm^2), $j_pE^0{}_{rev}$ the total power output, $j_p|E_{app}|$ the electrical power input and I_0 the power density of the incident light (100 mW/cm^2). $E^0{}_{rev}$ is the standard reversible potential which is 1.23 V/NHE, and the applied potential E_{app}= E_{meas}-E_{aoc}, where E_{meas} is the electrode potential (vs. Ag/AgCl) of the working electrode at which the photocurrent was measured under illumination and E_{aoc} is the electrode potential (vs. Ag/AgCl)

of the same working electrode at open circuit conditions, under the same illumination, and in the same electrolyte. The voltage at which the photocurrent becomes zero was taken as E_{aoc}.

The photocurrent density of $CdS/ZnIn_2S_4/TiO_2$ increases with increasing CdS deposition cycles, from 0 to 5, and then decreases while further increasing the deposition cycles. When the applied voltage was zero, the highest photocurrent 4.29 $mAcm^{-2}$ was achieved with the 5 cycles' CdS deposition, which is 4 and 14 times the photocurrent density obtained on $ZnIn_2S_4/TiO_2$ and bare TiO_2 NTA photoelectrodes, respectively. The lowest electron-hole recombination rate of the 5 cycles $CdS/ZnIn_2S_4/TiO_2$ can be attributed to the relatively smaller size of CdS nanoparticles. As shown in the inset of **Fig. 2F**, with increasing the deposition sequence, the CdS nanoparticles trend to aggregate. Although the loading amount increases at high deposition sequence, the particle number does not increase consequently but the particle size increases. The aggregated CdS particle may work as the hole-electron recombination centers due to the relatively big size and surface defects, [54, 55] which results in a decrease in the photo-conversion efficiency. Meanwhile, the photoconversion efficiencies measured for TiO_2 and $ZnIn_2S_4/TiO_2$ were 0.19% at -0.59 V vs. Ag/AgCl (**Fig. 5B**, curve a) and 0.38% at -0.70 V vs. Ag/AgCl (**Fig. 5B**, curve b), respectively. Deposition of CdS QDs significantly enhances the photoconversion efficiencies, with 2.0% at 0.74 V vs Ag/AgCl achieved on $CdS/ZnIn_2S_4/TiO_2$ with 5 cycles modification of CdS QDs, **Fig. 5B** (curve e).

Photocurrents increase with increasing applied potential up to 0 V for $ZnIn_2S_4/TiO_2$ (curve b) and $CdS(5)/ZnIn_2S_4/TiO_2$ (curve e) electrodes. Further increasing the applied potential, the photocurrent gets saturated, which can be attributed to the limitation of free photogenerated

electrons moving within the heterostructure or completely separation of the photogenerated electrons and holes under fixed light intensity. [56] As for TiO_2 NTAs (curve a) electrode, the photocurrents are much lower than those obtained on $ZnIn_2S_4/TiO_2$ and $CdS/ZnIn_2S_4/TiO_2$, and without saturation within the investigated potential range, indicating that construction of heterostructures $ZnIn_2S_4/TiO_2$ and $CdS/ZnIn_2S_4/TiO_2$ can enhance the absorption in the visible range and increase the photoelectrical conversion efficiency.

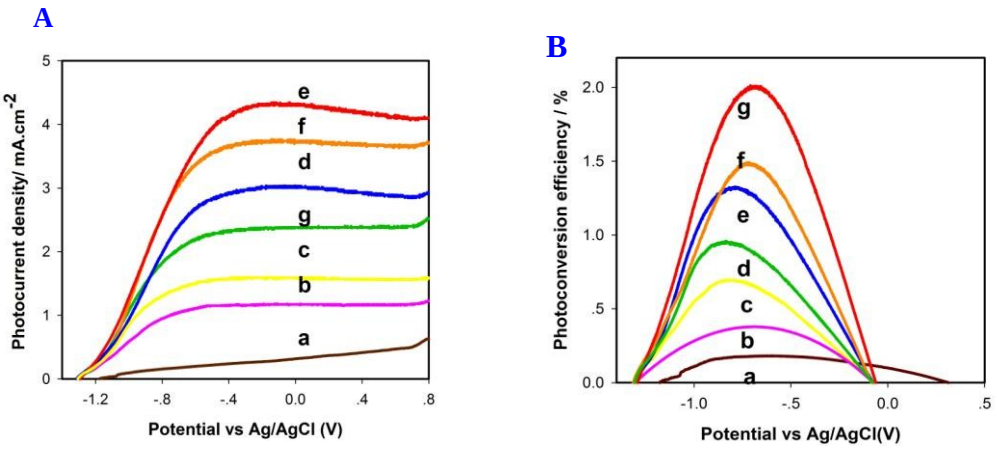

Fig.5. (A) Photocurrent density-voltage characteristics of unmodified TiO_2 (a), $ZnIn_2S_4/TiO_2$ (b) and $ZnIn_2S_4/TiO_2$ modified with 1 cycle (c), 3 cycles (d), 5 cycles (e), 7 cycles (f) and 9 cycles (g) of CdS QDs; (B) The corresponding photoconversion efficiencies under one sun illumination.

The electron-hole recombination characteristics were further studied by photoluminescence (PL), a widely used method to study surface structure, excited states and surface process involving electron/hole recombination.[47] The recombination of electron-hole pair emits photons resulting in photoluminescence.[57, 58] **Fig. 6** shows the PL spectra (excitation wavelength 275 nm) of the TiO_2 NTAs, $ZnIn_2S_4/TiO_2$, and $CdS/ZnIn_2S_4/TiO_2$ with different CdS amount expressed in deposition sequences. It can be observed that the $ZnIn_2S_4/TiO_2$ and

$CdS/ZnIn_2S_4/TiO_2$ heterostructures show lower PL intensity than the unmodified TiO_2 NTAs with the lowest PL intensity observed on the 5 cycles $CdS/ZnIn_2S_4/TiO_2$. The lower PL intensities of $ZnIn_2S_4/TiO_2$ and $CdS/ZnIn_2S_4/TiO_2$ heterostructures represent the fact that the emergence of the heterostructure results in a decrease in the recombination rate of electron-hole, and consequently an increase in the photoconversion efficiency.

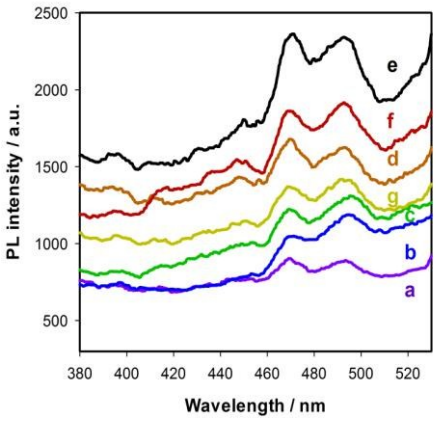

Fig.6. Room-temperature PL spectra of TiO_2 (a), $ZnIn_2S_4/TiO_2$ (b) and $ZnIn_2S_4/TiO_2$ modified with 1 cycle (c), 3 cycles (d), 5 cycles (e), 7 cycles (f) and 9 cycles (g) of CdS QDs.

The open-circuit dark-light-dark photovoltage response was measured to investigate recombination kinetics; the V_{oc} transient was monitored during relaxation from an illuminated quasi-equilibrium state to the dark equilibrium. [59]

Once the illumination on a photoelectrode at the open circuit is interrupted, the excess electrons are removed due to recombination, with the photovoltage decay rate directly related to the electron lifetime by the following expression:

$$\tau_n = [-k_B T/e][dV_{oc}/dt]^{-1} \quad (2)$$

where $k_B T$, e and dV_{oc}/dt are the thermal energy, positive elementary charge, and open-circuit voltage transient, respectively. Appropriate use of eq (2) assumes that the recombination is linear with a first-order dependence on electron concentration and that electron recombination occurs only with the electrolyte. [60]

Fig. 7A shows open-circuit dark-light-dark photovoltage responses of different photoelectrodes in an electrolyte containing 0.25 M Na_2S and 0.35 M Na_2SO_3 under illumination of 100 mW cm^{-2}. **Fig. 7B** is the plot of the response time obtained by applying eq (2) to the data in **Fig. 7A**. The photopotentials of $ZnIn_2S_4/TiO_2$ and $CdS/ZnIn_2S_4/TiO_2$ photoelectrodes are higher than those of the pure TiO_2 NTAs, indicating a greater accumulation of photogenerated electrons. The photopotential decays slowly after the photoelectrodes are returned to the dark indicating long $e\text{-}h^+$ lifetimes. In comparison to open circuit photovoltage decay measurement of the pure TiO_2 NTAs, the $CdS/ZnIn_2S_4/TiO_2$ exhibits better recombination characteristics, with the longer lifetimes indicating fewer recombination centers in the sample.

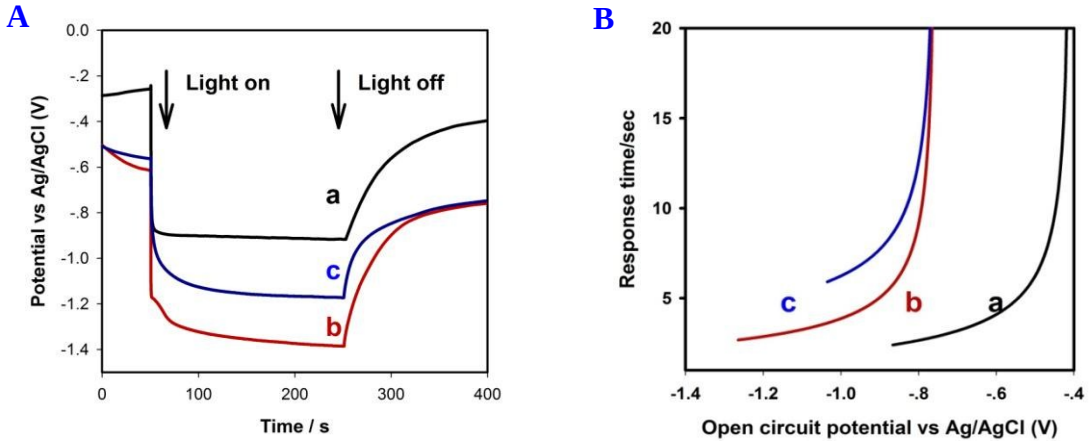

Fig.7. (A) The open-circuit photovoltage responses of TiO_2 (a), $ZnIn_2S_4/TiO_2$ (b) and $CdS/ZnIn_2S_4/TiO_2$ (c). (B) Response time determined by open-circuit potential decay for corresponding photoelectrodes shown in (A).

Photocatalytic activity

Photodegradation of 2, 4-D and MO solutions under visible light were performed to investigate the photocatalytic activities of $ZnIn_2S_4/TiO_2$ and $CdS/ZnIn_2S_4/TiO_2$ in comparison with those of the pure TiO_2 NTAs. Quantification was based on the optical absorption spectra of 2, 4-D and MO after visible light irradiation at different exposure times. Organic pollutants were determined following the Beer-Lambert's law for absorption band with the maximum at 227 nm for 2, 4-D and 464 nm for MO. The absorption peak under each spectrum was used to determine the quantity of pollutants degradation of each sample. As is shown in **Fig. 8A** and **8C**, after 140 min illumination, all characteristic peaks of MO disappear completely, indicating that the MO is completely degraded, while 90 min illumination degrades 2, 4-D completely, a performance comparable to that of other semiconductors. [61-64] As illustrated in **Fig.8B** and **8D**, under identical conditions, $CdS/ZnIn_2S_4/TiO_2$ shows a much higher activity than that of $ZnIn_2S_4/TiO_2$ and TiO_2.

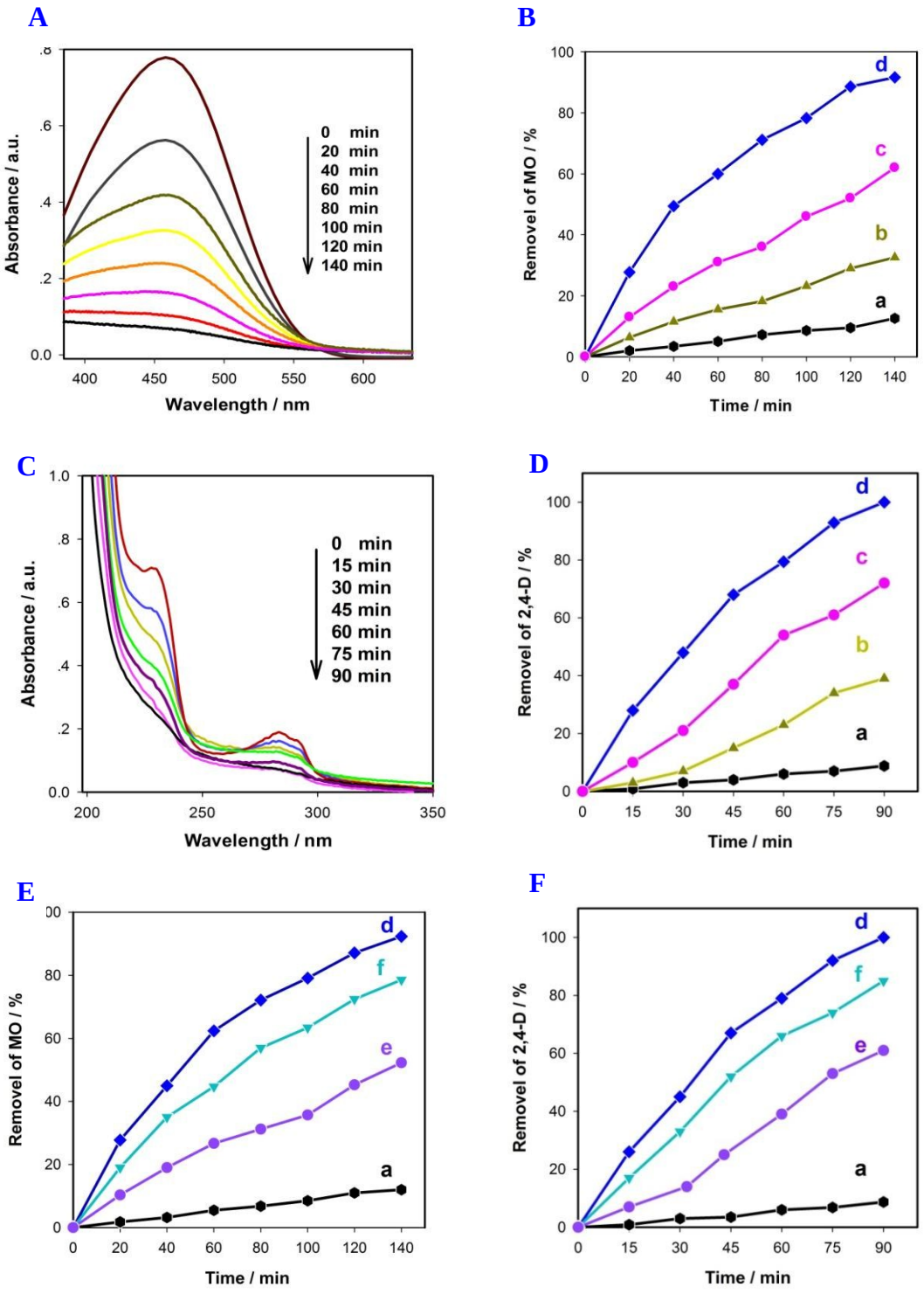

Fig.8. UV-vis determination of photoelectrocatalytic degradation of MO (A) and 2, 4-D (C). Corresponding photocatalytic performances of different photoelectrodes (B, D, E and F): (a) without catalyst, (b)TiO_2, (c) $ZnIn_2S_4/TiO_2$, (d) $CdS/ZnIn_2S_4/TiO_2$, (e) $ZnIn_2S_4$/Ti and (f) $CdS/ZnIn_2S_4$/Ti.

To further explore the function of TiO_2 NTAs during the photodegradation, contrast experiments were run by replacing TiO_2 NTAs with pure Ti sheet as the substrate. $ZnIn_2S_4$/Ti and CdS/$ZnIn_2S_4$/Ti were synthesized with the same method under the same conditions as preparing $ZnIn_2S_4/TiO_2$ and CdS/$ZnIn_2S_4/TiO_2$ with only replacing TiO_2 NTAs with pure Ti sheet as the substrate. Then the photodegradation of MO and 2, 4-D were performed under the same conditions to study the photocatalytic activities of $ZnIn_2S_4$/Ti and CdS/$ZnIn_2S_4$/Ti in comparison with those of CdS/$ZnIn_2S_4/TiO_2$. As shown in **Fig. 8E** and **8F**, under identical conditions, both $ZnIn_2S_4$/Ti and CdS/$ZnIn_2S_4$/Ti show lower activity than CdS/$ZnIn_2S_4/TiO_2$, suggesting that TiO_2 NTAs can promote electron transmission and charge separation.

Catalyst stability was evaluated by repeatedly measuring its efficiency in photoelectrocatalytic degradation of 2, 4-D and MO. The degradation rate of 2, 4-D with 90 min illumination decreases from 100% on the first run to 95.2 % on the fourth run (**Fig. 9A**). The degradation rate of MO with 140 min illumination is 91.7% on the first run, and 86.7 % on the fourth run (**Fig. 9B**). One may care about the chemical stability of the materials since photodegradation happens in the oxidative anode. For this reason, CdS/$ZnIn_2S_4/TiO_2$ were characterized by SEM and EDS after degradation process of 2, 4-D. As shown in **Fig. 9C** and **9D,** the structure of the material has little change, confirming the chemical stability.

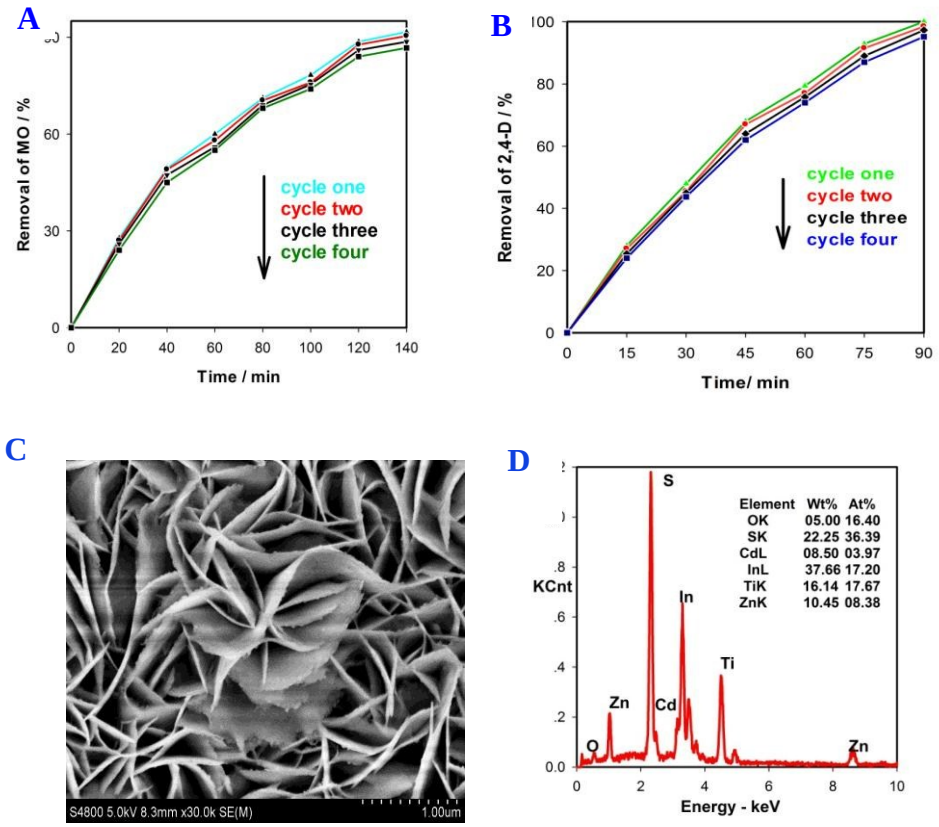

Fig.9. Photoelectrocatalytic stability of CdS/$ZnIn_2S_4$/TiO_2 on degradation of 2,4-D solution 90 min (A), MO solution after 140 min (B) under AM1.5G illumination; SEM (C) and EDS (D) of CdS/$ZnIn_2S_4$/TiO_2 composites after four cycles' degradation process.

Photodegradation Mechanism

Based on the previous reports [50, 65, 66] and the results mentioned above, a tentative photocatalytic degradation mechanism is proposed and is shown in **Fig. 10** with the following equations:

$$TiO_2 \rightarrow TiO_2(h^+ + e^-) \qquad ZnIn_2S_4 \rightarrow ZnIn_2S_4(h^+ + e^-) \qquad CdS \rightarrow CdS(h^+ + e^-) \qquad (3)$$

$$TiO_2(h^+ + e^-) + ZnIn_2S_4(h^+ + e^-) + CdS(h^+ + e^-)$$

$$\rightarrow TiO_2(e^-_{total}) + ZnIn_2S_4 + CdS(h^+_{total}) \quad (4)$$

$$TiO_2(e^-_{total}) + O_2 \rightarrow TiO_2 + \cdot O_2^- \quad (5)$$

$$H^+ + \cdot O_2^- \rightarrow \cdot O_2H \rightarrow\rightarrow 2 \cdot OH \quad (6)$$

$$CdS(h^+_{total}) + H_2O \rightarrow CdS + \cdot OH + H^+ \quad (7)$$

$$TiO_2(h^+ + e^-) \rightarrow TiO_2 \quad ZnIn_2S_4(h^+ + e^-) \rightarrow ZnIn_2S_4 \quad CdS(h^+ + e^-) \rightarrow CdS \quad (8)$$

$$\cdot OH + organic\ pollutants \rightarrow degradation\ products \quad (9)$$

Charge carriers are produced when photons are irradiated onto the photocatalyst in the suspended solution. The bandgap of TiO_2 (3.2 eV), $ZnIn_2S_4$ (2.6 eV) and CdS (2.4 eV) reduces progressively with the CB and VB increasing progressively to form a stepwise heterostructure that can absorb visible right. Under irradiation, photo-generated electrons are excited from the valence band (VB) to the conduction band (CB) of CdS, creating positive holes in the VB of CdS. Photo-excited electrons in the CB of CdS transfer to $ZnIn_2S_4$, and then migrating to TiO_2. Meanwhile, holes are transported in the opposite direction at the heterojunction interface. The separated electrons and holes migrate to the surface as reducing agents and sacrificial reagents, respectively (eq (3), eq (4)). Oxygen molecules dissolved in the suspension capture the electrons in the conduction band, and the holes in the valence band are captured by H_2O species adsorbed on the surface of the catalysts to produce the •OH radicals(eq (5), eq (6) and eq (7)), which subsequently degrades organic pollutants (eq (9)). [67, 68] Meanwhile, CB electrons may recombine with VB holes (eq (8)).

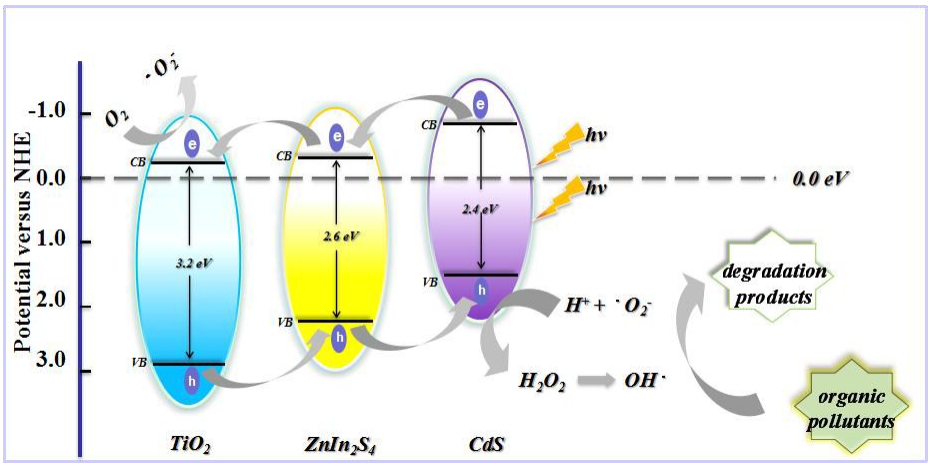

Fig.10. A schematic mechanism of the possible charge transfer in $CdS/ZnIn_2S_4/TiO_2$ heterojunction system.

To gain deeper insight into the charge transfer and recombination processes in $CdS/ZnIn_2S_4/TiO_2$ heterojunction electrode, the analysis of the formed •OH radical's on the sample surface under UV-Vis irradiation was performed by fluorescence technique with using TA, which readily reacted with •OH radicals to produce highly fluorescent product, 2-hydroxyterephthalic acid.[64, 67, 69-72] The intensity of the peak attributed to 2-hydroxyterephtalic acid was known to be proportional to the amount of •OH radicals formed. The selected concentration of TA solution was 5×10^{-4}M in a diluted NaOH aqueous solution with a concentration of 2×10^{-3} M. It has been proved that under these experimental conditions (low concentration of TA, less than 10^{-3} M, room temperature), the hydroxylation reaction of TA proceeds mainly by •OH radicals**.**

As shown in **Fig. 11A**, the PL intensity increases gradually with increasing irradiation time with $CdS/ZnIn_2S_4/TiO_2$ as photocatalyst, indicating OH is indeed formed during this photocatalytic process. To illustrate photocatalytic properties of different photoelectrodes, the PL

is recorded after irradiation 20 min, and the results are shown in **Fig. 11B**. From TiO_2 (curve c) to $CdS/ZnIn_2S_4/TiO_2$ (curve a), the PL intensity shows a gradual increase. The results confirm the best photocatalytic performance of $CdS/ZnIn_2S_4/TiO_2$.

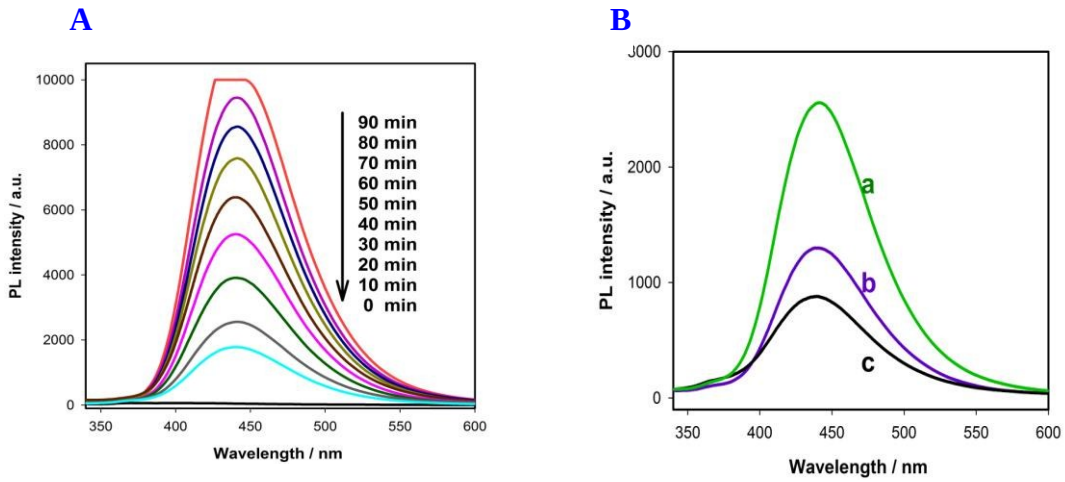

Fig.11. PL spectra measured during illumination with $CdS/ZnIn_2S_4/TiO_2$ (A) and different photoelectrodes (B): (a) $CdS/ZnIn_2S_4/TiO_2$, (b) $ZnIn_2S_4/TiO_2$ and (c) TiO_2 .

Conclusions

A novel $CdS/ZnIn_2S_4/TiO_2$ heterostructure is prepared by a mild hydrothermal method combined with a SILAR technique. The photoelectrical performances of the as prepared materials are carefully investigated; optimal samples demonstrate a solar spectrum photoconversion efficiency of approximately 2.0%. Photocatalytic performance was tested by photodegradation of organic pollutants, with excellent efficiencies obtained; a photodegradation mechanism was proposed on the basis of band alignment to elucidate the enhancement of efficiency seen in the $CdS/ZnIn_2S_4/TiO_2$ material system.

Experimental section

Materials and chemicals

Titanium foil (99.8% purity, 0.25 mm thick) was purchased from Aldrich (Milwaukee, WI). Zinc sulfate heptahydrate($Zn_2SO_4 \cdot 7H_2O$), indium(III) chloride tetrahydrate ($InCl_3$) and thioacetamide (TAA) (99.0%) were commercially available from Aladdin (Shanghai). Methyl orange (MO) and 2, 4-D was obtained from Shanghai Chemical Corporation of China. All other reagents of analytical reagent (AR) grade were obtained from commercial sources and used as received without any further purification.

All experiments, excluding those with special annotation, were conducted at room temperature. Ultrapure water was prepared with Mill-Q water (Millipore, 18.2 MΩ resistivity) and used throughout the experiment.

Apparatus

The morphologies of the prepared materials were analyzed using a field-emission scanning electron microscope (FE-SEM, Hitachi S-4800). An energy dispersive X-ray spectrometer (EDS) fitted to the field-emission scanning electron microscope was used to identify elemental composition of the product. PL spectra were recorded using a Hitachi F-4600 fluorescence spectrophotometer (Tokyo, Japan). The UV-vis diffuse reflectance spectra of the samples were measured by using an UV-vis spectrophotometer (Cary 300, Varian, USA) with a

150 mm integrating sphere. UV-vis absorbance spectra were measured by using an UV-Vis spectrophotometer (Cary 60, Agilent, USA).

Fabrication of the TiO_2 NTAs

Titanium ribbons were cleaned in 3% hydrofluoric acid (30 seconds), rinsed with deionized water, ultrasonic cleaned for 5 min in acetone solution and ethanol, and then dried in a nitrogen stream prior to anodization. The cleaned titanium ribbon was anodized at 20 V constant voltage for 2 h using a two-electrode electrochemical cell with a platinum foil counter electrode in electrolyte containing 0.5 M $NaHSO_4$ and 0.1 M NaF at room temperature. To induce high crystallinity, the highly ordered TiO_2 NTAs were annealed at 500℃ for 3 h with heating and cooling rates of 2℃/min.

Preparation of $ZnIn_2S_4$ nanosheet/TiO_2 NTAs heterostructure

$ZnIn_2S_4$ nanosheet/TiO_2 NTAs heterostructures were synthesized by a facile hydrothermal method. Briefly, 25 mM of $Zn_2SO_4 \cdot 7H_2O$, 50 mM of $InCl_3$, 100 mM of TAA and 10 mL of ultrapure water were loaded into a Teflon-lined stainless steel autoclave with 20 mL capacity and stirred for 30 min. The TiO_2 NTAs was put on the bottom of the Teflon-liner of autoclave. After that, the autoclave was sealed, maintained at 150℃ for 15 min, and cooled down to room temperature naturally. A layer of yellow film was deposited on the TiO_2 substrate, clearly visible to the unaided eye. Once washed by ultrapure water and ethanol, the sample was dried at 60℃ for 2 h under vacuum.

Preparation of CdS/$ZnIn_2S_4$/ TiO_2 heterostructures

CdS is deposited onto the $ZnIn_2S_4/TiO_2$ heterostructures by a successive ionic layer adsorption and reaction (SILAR) process.[73] Briefly, 0.5 M cadmium nitrate in ethanol was used as the cation source and 0.5 M sodium sulfide in 1:1 methanol and water as the anion source. The sample was dipped into cation source for 5 min, rinsed with ethanol, then dipped for another 5 min into anion source and again rinsed with methanol. The two-step dipping procedure is termed as one SILAR cycle and the procedure was repeated until a desired deposition of CdS nanocrystalline was achieved. Finally, the photoelectrode was dried in a nitrogen stream, then annealed at 350℃ in N_2 atmosphere for 60 min.

Photoelectrochemical activity measurement

Photoelectrochemical (PEC) measurements were conducted using an electrochemical workstation (CHI660D, Shanghai Chenhua Instrument Co. Ltd.) in a standard three-electrode configuration with a CdS/$ZnIn_2S_4/TiO_2$ sample, 1.0 cm^2 in area, as the working electrode, a Pt wire counter electrode and an Ag/AgCl reference electrode. A 500W xenon lamp (CHFXQ-500 W, Beijing Changtuo Co., Ltd.), filtered to 100 $mWcm^{-2}$ AM1.5G as determined by a radiometer (NOVA Oriel 70260), was used as the light source. An aqueous solution containing 0.35M Na_2SO_3 and 0.24 M Na_2S served as the PEC electrolyte.

Photocatalytic activity measurement

The photocatalytic activity of the $CdS/ZnIn_2S_4/TiO_2$ was evaluated by degradation of organic pollutants including 20 mg/L 2, 4-D and MO in 20 mL 0.05 M Na_2SO_4, with tests carried out under constant stirring. The organic composition solution to be photo-degraded was left in the dark for 30 min prior to irradiation to achieve absorption equilibrium. Then steady-state photolysis was carried out in a 20 mL optical quartz cell. The concentration change during the degradation procedure was monitored by determining the UV-vis adsorption of 60 μL of sample taken from the solution. After measurement, the solution was immediately added back to the reaction cell to keep the volume constant. The degree of organic compound degradation was defined as follows:

$$Removal\ efficiency\ = (C_0 - C_t)/C_t \times 100\% \ = (A_0 - A_t)/A_t \times 100\% \quad (10)$$

Where C_0 is the initial concentration measured after stirring for 30 min in the dark, and C_t the residual concentration measured after illumination of time t. Assuming the absorbance A is linear related to the concentration in the investigated range, C_t and C_0 can be represented with corresponding A_t and A_0.

Analysis of photodegradation mechanism.

Hydroxyl radicals (OH) produced by the as-prepared photoelectrode under AM 1.5G illumination were detected by the PL analysis using TA as probe molecule. Experimental steps were similar to those of the degradation procedure except that organic pollutant solution is

replaced by the 5×10^{-4} M TA and 2×10^{-3} M NaOH. The change of $\cdot OH$ concentration during the degradation procedure was monitored by determining the fluorescence emission intensity with an excitation wavelength of 320 nm.

ACKNOWLEDGMENTS

The authors are thankful to the National Science Foundation of China under the grant (21175038, 21235002) for providing financial support.

REFERENCES

1. M.R. Hoffmann, S.T. Martin, W. Choi and D.W. Bahnemann, *Chem. Rev.*, 1995, **95,** 69-96.
2. A. Mills and S.L. Hunte, *J. Photoch. Photobiol. A*, 1997, **108,** 1-36.
3. T. Nakashima and N. Kimizuka, *J. Am. Chem. Soc.*, 2003, **125**, 6386-6387.
4. A. Azam, F. Ahmed, N. Arshi, M. Chaman and A. Naqvi, *J. Alloy. Compound.*, 2010, **496**, 399-402.
5. H. Zhu, J. Wang and G. Xu, *Cryst. Growth Des.*, 2008, **9**, 633-638.
6. G. Li, S. Yan, Z. Wang, X. Wang, Z. Li, J. Ye and Z. Zou, *J. Chem. Soc., Dalton Trans.*, 2009, **40**, 8519-8524.
7. G. Huang and Y. Zhu, *Mater. Sci.Eng. B*, 2007, **139**, 201-208.
8. R. Ramakrishnan, S. Kalaivani, J. Amala Infant Joice and T. Sivakumar, *Appl. Surf. Sci.*, 2012, **258**, 2515-2521.
9. C.J. Zhao, B. Feng, Y.T. Li, J. Tan, X. Lu and J. Weng, *Appl. Surf. Sci.*, 2013, **280**, 8-14.
10. M. lamal, J.M. Macak, P. chmuki and J. Kry'saa, *Electrochem. Commun.*, 2007, **9**, 2822-2826.
11. F. Quan, Y. Hu, X. Zhang and C. Wei, *Appl. Surf. Sci.*, 2014, **320**, 120-127.
12. Q. Huang, S. Tian, D. Zeng, X. Wang, W. Song, Y. Li, W. Xiao and C. Xie, *ACS catal.*, 2013, **3**, 1477-1485.
13. Z. Liu, X. Zhang, S. Nishimoto, M. Jin, D. A. Tryk, T. Murakami and A. Fujishima, *J. Phys. Chem. C*, 2008, **112**, 253-259.

14. R. Zhou, Q. Zhang, E. Uchaker, J. Lan, M. Yin and G. Cao, *J. Mater. Chem. A*, 2014, **8**, 2517-2525.

15. L. Yang, C. McCue, Q. Zhang, E. Uchaker, Y. Mai and G. Cao, *Nanoscale*, 2015, **7**, 3173-3180.

16. B. Liu, L. M. Liu, X. F. Lang, H. Y. Wang, X. W. D. Lou and E. S. Aydil, *Energ. Environ. Sci.*, 2014, **7**, 2592-2597.

17. H. B. Yang, J. Miao, S. F. Hung, F. Huo, H. M. Chen and B. Liu, *ACS Nano*, 2014, **8**, 10403-10413.

18. S. Sakthivel and H. Kisch, *Angew. Chem. Int. Ed.*, 2003, **42**, 4908-4911.

19. A. Naldoni, M. Allieta, S. Santangelo, M. Marelli, F. Fabbri, S. Cappelli, C. L. Bianchi, R. Psaro and V. Dal Santo, *J. Am. Chem. Soc.*, 2012, **134**, 7600-7603.

20. W. Zhou, H. Liu, J. Wang, D. Liu, G. Du and J. Cui, *ACS Appl. Mater. Inter.*, 2010, **2**, 2385-2392.

21. J.J. Lin, J.X. Shen, R.J. Wang, J.J. Cui, W.J. Zhou, P.G. Hu, D. Liu, H.Liu, J.Y. Wang, R.I. Boughton and Y.Z. Yue, *J. Mater. Chem.*, 2011, **21**, 5106-5113.

22. J. Tian, Y.H. Sang, Z.H. Zhao, W.J. Zhou, D.Z. Wang, X.L. Kang, H. Liu, J.Y. Wang, S.W. Chen, H.Q. Ca and H. Huang, *Small*, 2013, **9**, 3864-3872.

23. J. Tian, Y.H. Sang, G.W. Yu, H.D. Jiang, X.N. Mu and H. Liu, *Adv. Mater.*, 2013, **25**, 5075-5080.

24. X.D. Wang, Z.D. Li, J. Shi and Y.H. Yu, *Chem. Rev.*, 2014, **114**, 9346-9384.

25. X.F. Gao, W.T. Sun, Z.D. Hu, G. Ai, Y.L. Zhang, S. Feng, F. Li and L.M. Peng, *J. Phys. Chem. C*, 2009, **113**, 20481-20485.

26. Y.L. Lee, C.F. Chi and S.Y. Liau, *Chem. Mater.*, 2010, **22**, 922-927.

27. X.F. Gao, H.B. Li, W.T. Sun, Q. Chen, F.Q. Tang and L.M. Peng, *J. Phys. Chem. C*, 2009, **113**, 7531-7535.

28. K.P. Acharya, T.R. Alabi, N. Schmall, N.N. Hewa-Kasakarage, M. Kirsanova, A. Nemchinov, E. Khon and M. Zamkov, *J. Phys. Chem. C*, 2009, **113**, 19531-19535.

29. L. Ge, J. Liu, *Appl. Catal. B*, 2011, **105**, 289-297.

30. H.N. Kim, T.W. Kim, I.Y. Kim and S.J. Hwang, *Adv. Funct. Mater.*, 2011, **21**, 3111-3118.

31. X.W. Wang, G. Liu, Z.G. Chen, F. Li, L.Z. Wang, G.Q. Lu and H.M. Cheng, *Chem. Commun.*, 2009, **23**, 3452-3454.

32. J.G. Hou, Z. Wang, W.B. Kan, S.Q. Jiao, H.M. Zhu and R.V. Kumar, *J. Mater. Chem.*, 2012, **22**, 7291-7299.

33. X.L. Hu, J.C. Yu, J.M. Gong and Q. Li, *Cryst. Growth Des.*, 2007, **7**, 2444-2448.

34. F. Fang, L. Chen, Y.B. Chen and L.M. Wu, *J. Phys. Chem. C*, 2010, **114**, 2393-2397.

35. N. Romeo, A. Dallaturca, R. Braglia and G. Sberveglieri, *Appl. Phys. Lett.*, 1973, **22**, 21-22.

36. B. Chai, T.Y. Peng, P. Zeng, X.H. Zhang and X.J. Liu, *J. Phys. Chem. C*, 2011, **115**, 6149-6155.

37. Z.X. Chen, D.Z Li, W.J Zhang, Y. Shao, T.W Chen, M. Sun and X.Z. Fu, *J. Phys. Chem. C*, 2009, **113**, 4433-4440.

38. W.S. Seo, R. Otsuka, H. Okuno, M. Ohta and K. Koumoto, *J. Mater. Res.*, 1999, **14**, 4176-4181.

39. Z.B. Lei, W.S. You, M.Y. Liu, G.H. Zhou, T. Takata, M. Hara, K. Domen and C. Li, *Chem. Commun.*, 2003, **17**, 2142-2143.

40. Q. Li, B.D. Guo, J.G. Yu, J.R. Ran, B.H. Zhang, H.J. Yan and J.R. Gong, *J. Am. Chem. Soc.*, 2011, **133**, 10878-10884.

41. Q. J. Xiang, J. G. Yu and M. Jaroniec, *J. Am. Chem. Soc.*, 2012, **134**, 6575-6578.

42. J. Zhang, J.G. Yu, Y.M. Zhang, Q. Li and J.R. Gong, *Nano Lett.*,2011, **11**, 4774-4779.

43. B. Chai, T.Y. Peng, P. Zeng and X.H. Zhang, *Dalton Trans.*, 2012, **41**, 1179-1186.

44. S.J. Peng, P.N. Zhu, S.G. Mhaisalkar and S. Ramakrishna, *J. Phys. Chem. C*, 2012, **116**, 13849-13857.

45. L.X. Yang and Q.Y. Cai, *Inorg. Chem.*, 2006, **45**, 9616-9618.

46. Q.Y. Cai, M. Paulose, O.K. Varghese and C.A. Grimes, *J. Mater. Res.*, 2005, **20**, 230-236.

47. A. Kongkanand, K. Tvrdy, K. Takechi, M. Kuno and P.V. Kamat, *J. Am. Chem. Soc.*, 2008, **130** 4007-4015.

48. Q. Liu, H. Lu, Z.W. Shi, F.L. Wu, J. Guo, K. Deng and L. Li, *ACS Appl. Mater. Inter.*, 2014, **6**, 17200-17207.

49. J.G. Hou, C. Yang, H.J. Cheng, Z. Wang, S.Q. Jiao and H.M. Zhu, *Phys. Chem. Chem. Phys.*, 2013, **15**, 15660-15668.

50. M.A. Mahadik, P.S. Shinde, M. Cho and J.S. Jang, *J. Mater. Chem. A*, 2015, **00**, 1-9.

51. G.M. Wang, X.Y. Yang, F. Qian, J.Z. Zhang and Y. Li, *Nano Lett.*, 2010, **10**, 1088-1092.

52. O.K. Varghese and C.A. Grimes, *Sol. Energy Mater. Sol. Cells*, 2008, **92**, 374-384.

53. S. U. M. Khan, M. Al-Shahry and W.B. Ingler, *Science*, 2002, **297**, 2243-2245.

54. Q. Kang, Q.Z. Lu, S.H. Liu, L.X. Yang, L.F. Wen, S.L. Luo and Q.Y. Cai, *Biomaterials*, 2010, **31**, 3317-3326.

55. H. Feng, T.T. Tran. T, L. Chen, L.J. Yuan and Q.Y. Cai, *Chem. Eng. J.*, 2013, **215-216**, 591-599.

56. X. Nie, J.Y. Chen, G.Y. Li, H.X. Shi, H.J. Zhao, P.K. Wong and T.C. An, *J. Chem. Technol. Biot.*, 2013, **88**, 1488-1497.

57. Y. Cong, J. Zhang, F. Chen, M. Anpo and D. He, *J. Phys. Chem. C*, 2007, **111**, 10618-10623.

58. G. Liu, F. Li, Z. Chen, G.Q. Lu and H.M. Cheng, *J. Solid State Chem.*, 2006, **179**, 331-335.

59. A. Zaban, M. Greenshtein and J. Bisquert, *Chem. Phys. Chem.*, 2003, **4**, 859-864.

60. G.K. Mor, K. Shankar, M. Paulose, O.K. Varghese and C.A. Grimes, *Nano Lett.*, 2006, **6**, 215-218.

61. J. Bisquert, A. Zaban, M. Greenshtein and I. Mora-Seró, *J. Am. Chem. Soc.*, 2004, **126**, 13550-13559.

62. L. Chen, T.T. Tran. Ta, C.A. Huang, J.Z. Li, L.J. Yuan and Q.Y. Cai, *Appl. Surf. Sci.*, 2013, **273**, 82-88.

63. T.T. Tran. T, P.T. Sheng, C.A. Huang, J.Z. Li, L. Chen, L.J. Yuan, C.A. Grimes and Q.Y. Cai, *Chem. Eng. J.*, 2010, **210**, 425-431.

64. W.L. Li, P.T. Sheng, H.Y. Feng, X.H. Yin, X.W. Zhu, X. Yang and Q.Y. Cai, *ACS Appl. Mater. Inter.*, 2014, **6**, 12353-12362.

65. S.M. Yang, C.H. Huang, J. Zhai, Z.S. Wang and L. Jiang, *J. Mater. Chem.*, 2002, **12**, 1459-1464.

66. P.T. Sheng, W.L. Li, J. Cai, X. Wang, X. Tong, Q.Y. Cai and C.A. Grimes, *J. Mater. Chem. A*, 2013, **1**, 7806-7815.

67. Z.M. Wu, X. Tong, P.T. Sheng, W.L. Li, X.H. Yin, J.M. Zou and Q.Y. Cai. *Appl. Surf. Sci.*, 2015, **351**, 309-315.

68. C. C. Hu, T. C. Hsu and S. Y. Lu, *Applied Surface Science*, 2013, **280**, 171-178.

69. A. Houas, H. Lachheb, M. Ksibi, E. Elaloui, C. Guillard and J.M. Herrmann, *Appl. Catal. B,* 2001, **31**, 145-157.

70. K. Ishibashi, A. Fujishima, T. Watanabe and K. Hashimoto, *Electrochem. Commun.*, 2000, **2**, 207-210.

71. Q. Xiao, Z.C. Si, J. Zhang, C. Xiao and X.K. Tan, *J. Hazard. Mater.*, 2008, **150,** 62-67.

72. J.G. Yu, W.G. Wang, B. Cheng and B.L. Su, *J. Phys. Chem. C, 2009,* **113,** 6743-6750.

73. K. Prabakar, H. Seo, M. Son and H. Kim, *Mater. Chem. Phys.*, 2009, **117**, 26-28.

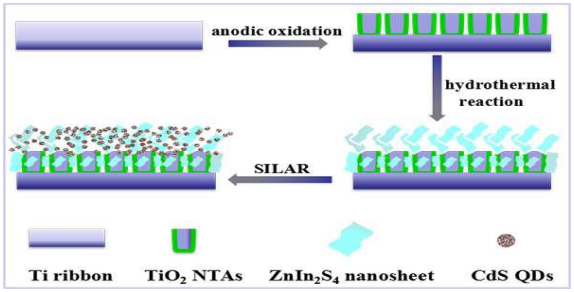

A $CdS/ZnIn_2S_4/TiO_2$ 3D-heterostructure with high photoconversion efficiency and photocatalytic activity was synthesized and applied.